Supplementary Figures

Perovskite types and synthetic methods

The structure of the perovskite photodetector prepared in this article is as follows: FTO/c-TiO_2/m-TiO_2/PVK. The PVK component is $MAPbI_3$.

The synthesis method of perovskite is as follows. By mixing PbI_2, MAI and SiW_9Co_3@rGO to prepare the perovskite precursor (1 mL). The solvent used the mixed solution, which the volume ratio of N,N-dimethylformamide (DMF) and dimethyl sulfoxide (DMSO) is 4:1. The optimized perovskite film was prepared by dropping the solution (80 μL) on the substrate and the device was spun at 2000 rpm for 30 s at an acceleration of 500 rpm/s, then the annealing was done by placing the device on a hot plate at 70 ℃ for 30 minutes.

Characterization and measurements

Crystal structures of as-obtained products were characterized by XRD recorded on a Bruker AXS diffractometer using Cu Kα radiation. Fourier transform infrared (FTIR) spectra were obtained on a BRUKE Vertex 70 spectrometer using KBr pellets. Raman spectra were recorded on a microscopic confocal Raman spectrometer (Horiba JobinYvon, LabRAM HR) with an excitation of 532 nm laser light. Morphologies and microstructures of the products were characterized by scanning electron microscopy (SEM) (Hitachi SU-8010) equipped with an Energy Dispersive Spectrometer (EDS) and transmission electron microscopy (TEM) images were obtained using a Philips Tecnai 20U-Twin microscope at an acceleration voltage of 200 kV. (JEOL JEM-2100F). The diffuse reflectance spectroscopy (DRS) of the products were recorded by Shimadzu UV 2600 spectrophotometer equipped with an integrating sphere, using 100% $BaSO_4$ as reflectance standard. The UV-visible spectroscopy of the products were recorded by Hitachi U-3010, the wavelength range is 300-800 nm. X-ray photoelectron spectroscopy (XPS) measurement was performed using a Thermo Scientific Escalab 250Xi spectrometer with monochromatized Al Kα excitation. The photoluminescence (PL) spectra were measured using FLSP920 fluorospectro photometer at 467 nm laser excitation at room temperature, decay curves were fitted by

a bi-exponential decay function to obtain deconvolution of the instrument response function. Cyclic voltammetry (CV) were performed using a CHI601D electrochemical workstation (Shanghai Chenhua) with a three-electrode system containing a GCE as the working electrode (WE), a Pt coil as the counter electrode (CE), and an Ag coil as the quasi-reference electrode (RE). The voltage of the photomultiplier tube (185–850 nm) was biased at 800 V. The linear voltammetry curve was measured by Corr Test CS electrochemical workstation, and the sweep speed was 50 mV/s. The I-T curve and I-V curve was tested by Gamry Electrochemical workstation at room temperature with a bias of 3V and a Xenon light source model XQ-500W.

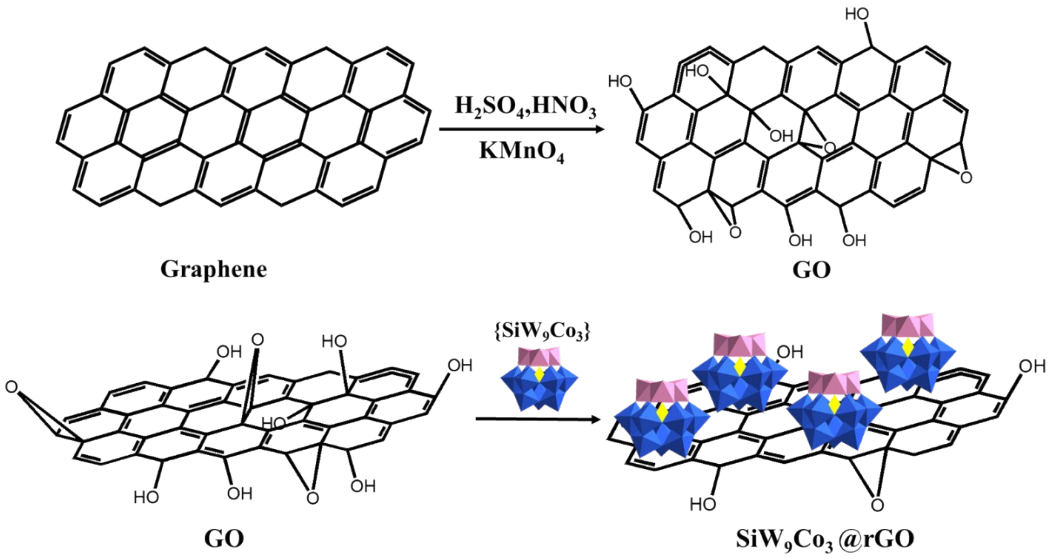

Figure S1. Schematic diagram of the synthesis of SiW_9Co_3@rGO.

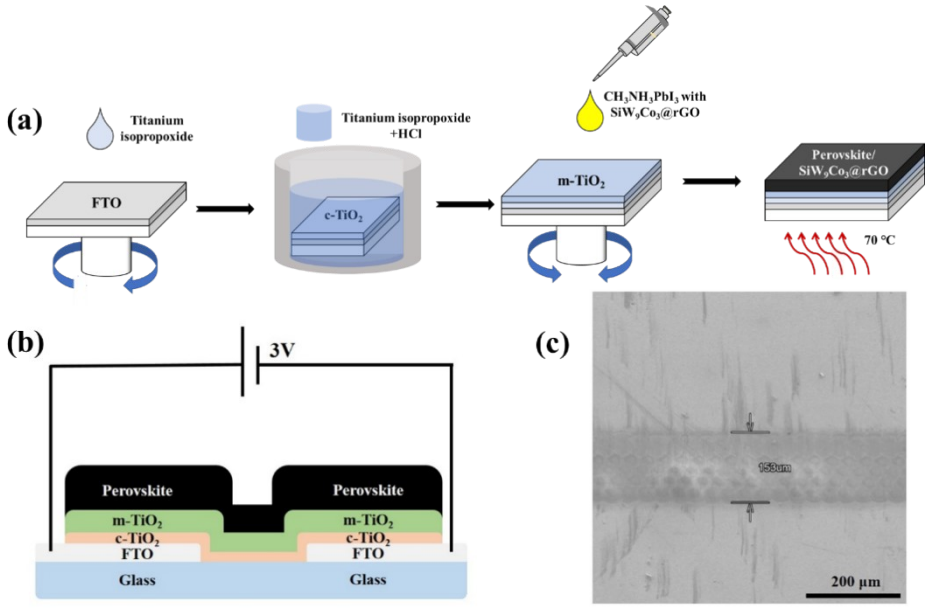

Figure S2. (a) Manufacturing process of perovskite photodetectors and (b) structure of the photodetector, where c-TiO_2 represents compact TiO_2 layer and m-TiO_2 represents mesoporous TiO_2 layer; (c) SEM image of the top surface of FTO.

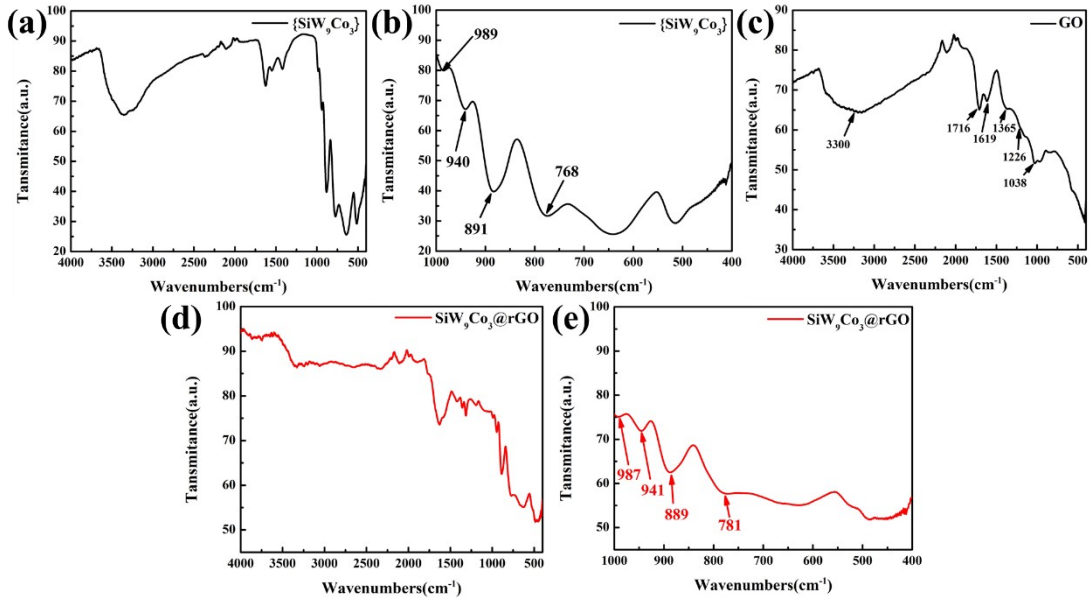

Figure S3. IR of $\{SiW_9Co_3\}$, GO, and SiW_9Co_3@rGO.

Note: At 3300 cm^{-1} and 1365 cm^{-1}, there are vibration and deformation peaks of the O-H bond. At 1716 cm^{-1}, there is an epoxy based C-O absorption peak. At 1619 cm^{-1}, there is a C=C stretching vibration peak similar to the benzene ring structure. At 1226 cm^{-1} and 1038 cm^{-1}, there are vibration absorption peaks of C-O-C. The C-H bending vibration peak is located at 780 cm^{-1}.

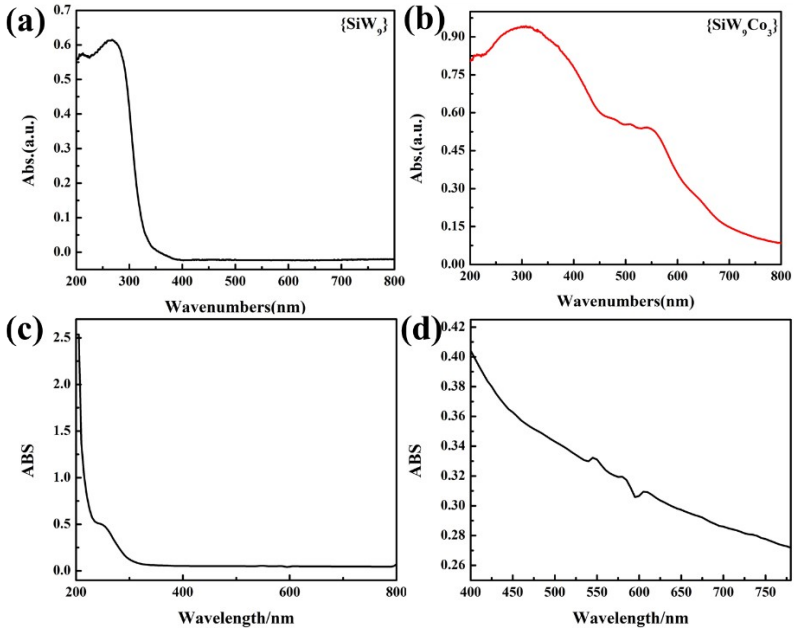

Figure S4. (a) Solid UV-vis absorption spectrum of $\{SiW_9\}$; (b) Solid UV-vis absorption spectrum of $\{SiW_9Co_3\}$; (c), (d) Liquid UV-vis absorption spectrum of $\{SiW_9Co_3\}$.

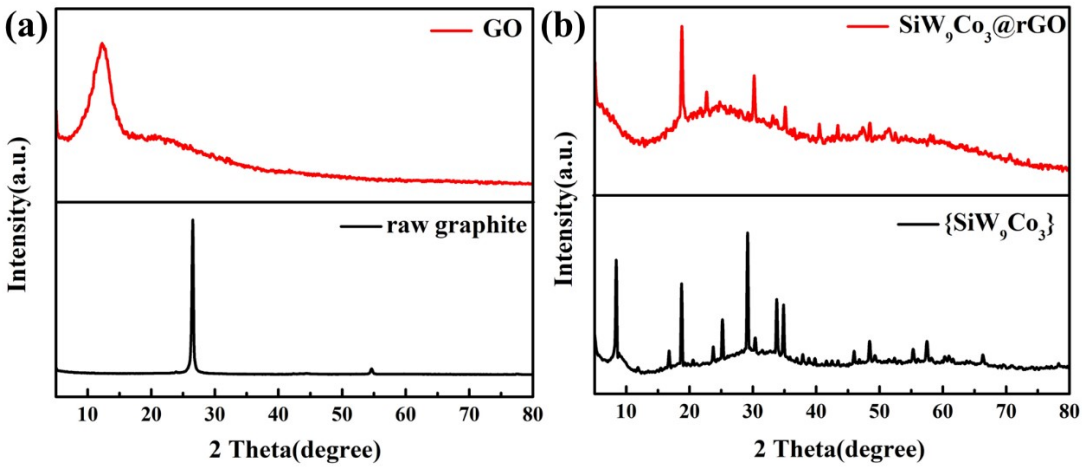

Figure S5. (a) XRD patterns of raw graphite and GO; (b) XRD patterns of $\{SiW_9Co_3\}$ and SiW_9Co_3@rGO.

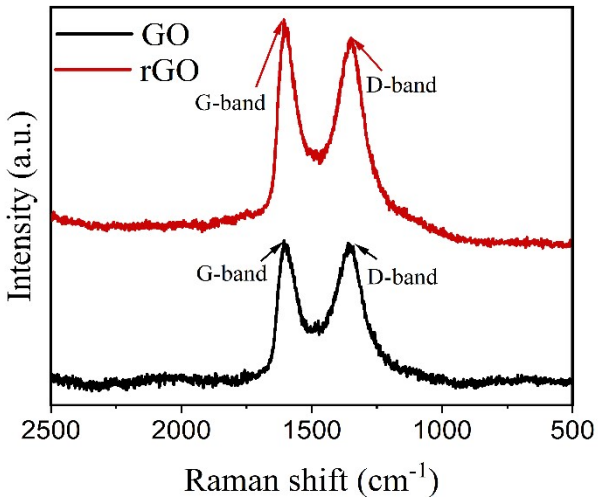

Figure S6. XRD patterns of raw graphite and GO.

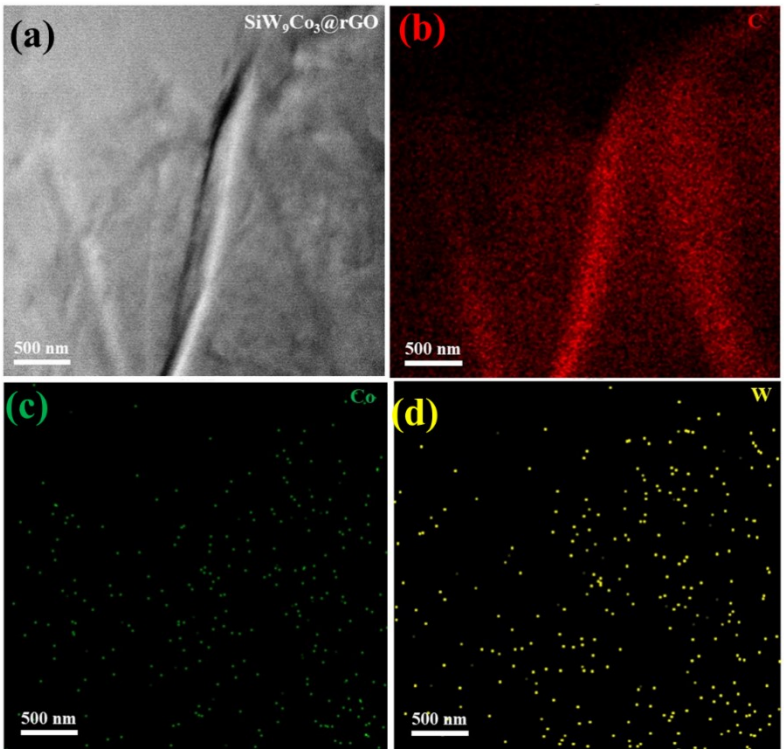

Figure S7. (a) TEM image of SiW_9Co_3@rGO; elemental mapping images of (b) C, (c) Co and (d) W in SiW_9Co_3@rGO.

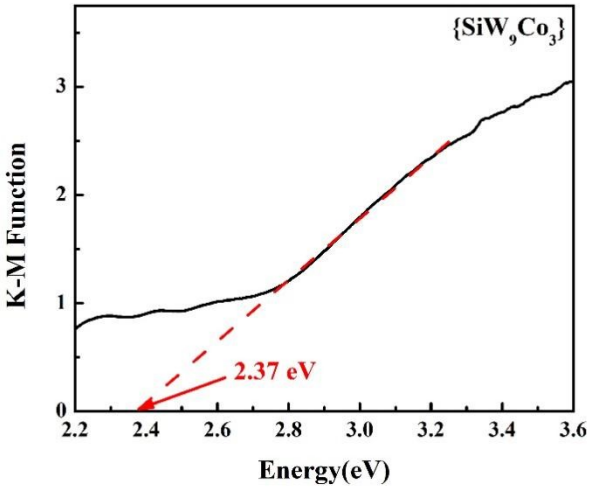

Figure S8. The Kubelka-Munk function of $\{SiW_9Co_3\}$ versus its energy E curve.

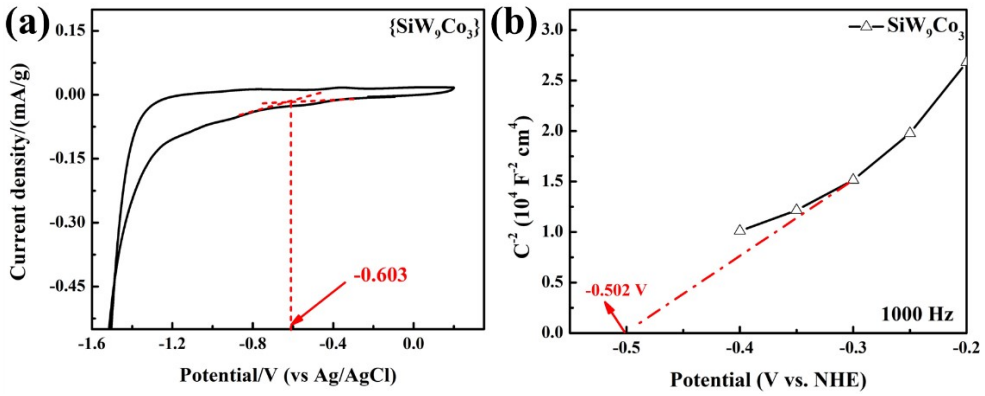

Figure S9. (a) C-V curve of {SiW_9Co_3}; (b) Mott-Schottky curve of {SiW_9Co_3}

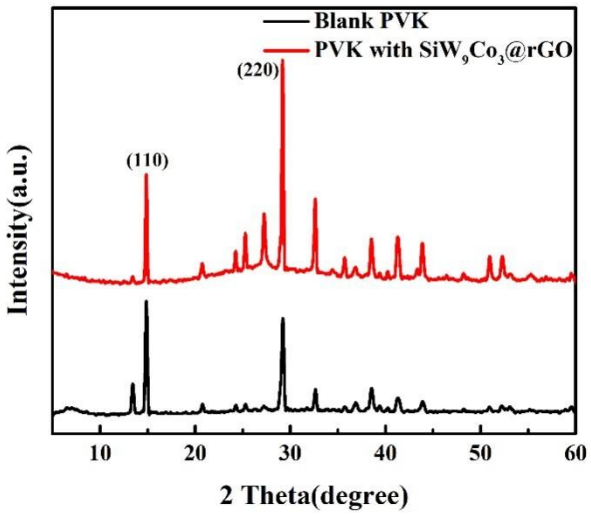

Figure S10. XRD patterns of blank perovskite and doped SiW_9Co_3@rGO.

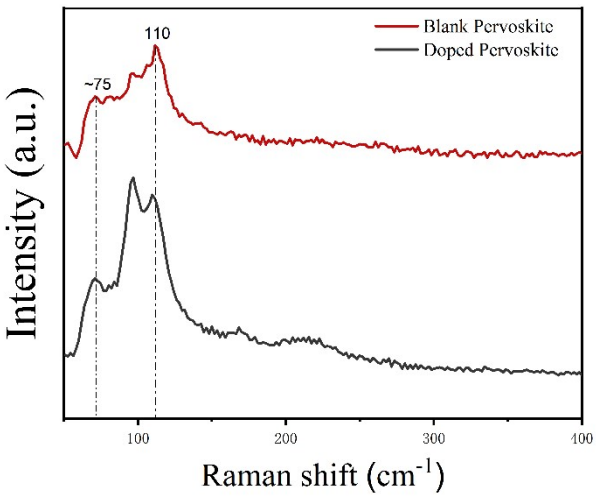

Figure S11. Raman patterns of blank perovskite and doped SiW_9Co_3@rGO.

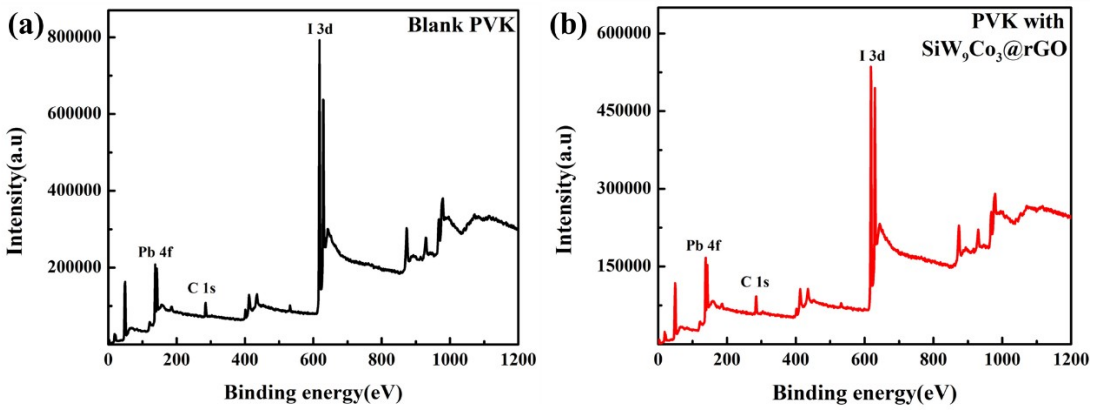

Figure S12. (a) XPS spectrum of blank perovskite; (b) XPS spectrum of perovskite doped with SiW_9Co_3@rGO.

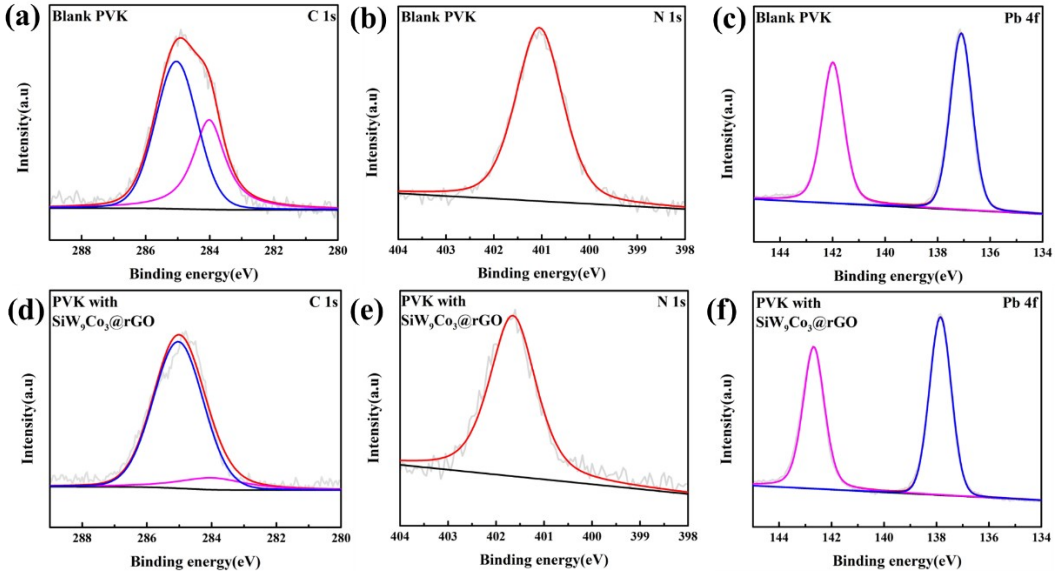

Figure S13. High-resolution energy spectra of (a) C 1s, (b) N 1s, and (c) Pb 4f of blank perovskite; High-resolution energy spectra of (d) C 1s, (e) N 1s, and (f) Pb 4f of perovskite doped with SiW_9Co_3@rGO.

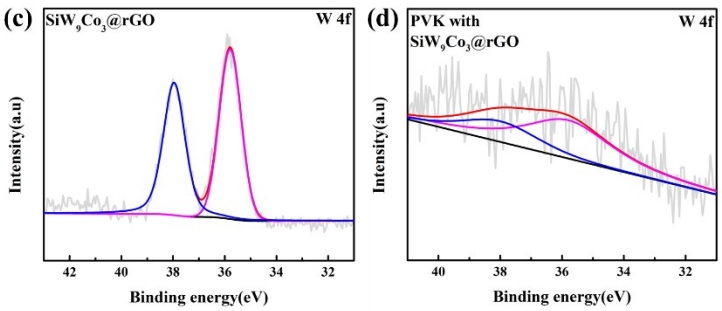

Figure S14. W 4f high-resolution energy spectra of (a) SiW_9Co_3@rGO and (b) perovskite doped with SiW_9Co_3@rGO.

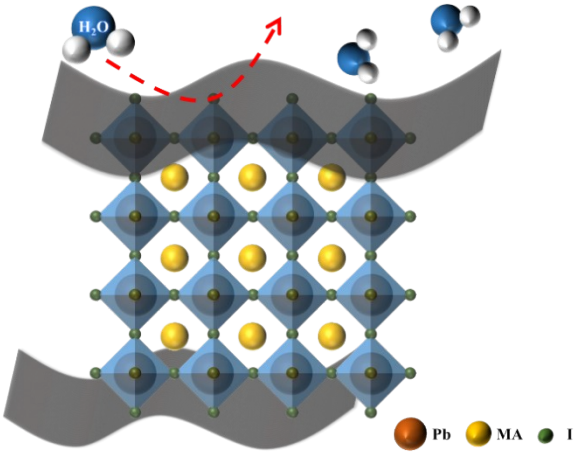

Figure S15. Diagram of the mechanism of SiW_9Co_3@rGO improving the stability in perovskite photodetectors.

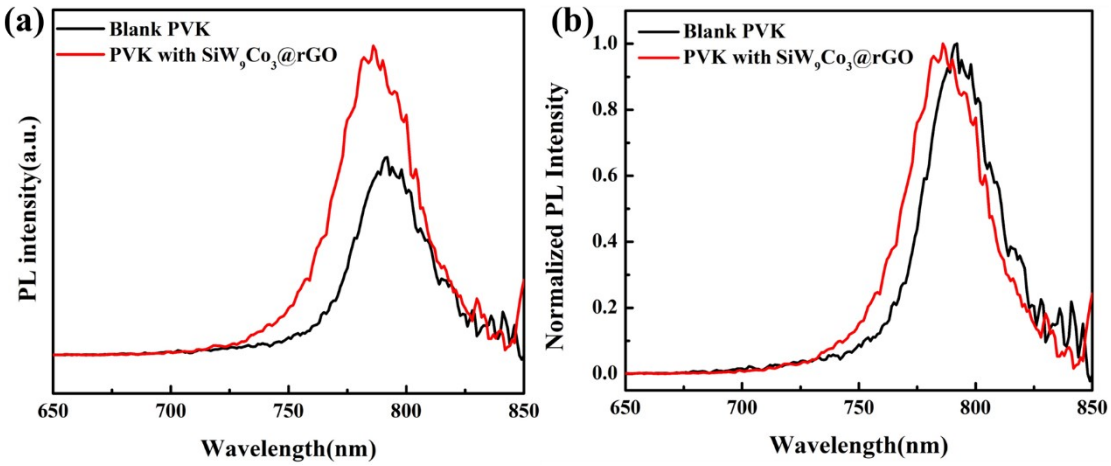

Figure S16. (a) Fluorescence spectra and (b) normalized spectra of blank perovskite photodetectors and photodetectors doped with SiW_9Co_3@rGO.